Int J Mech Mater Des
https://doi.org/10.1007/s10999-020-09524-8

Numerical and experimental analysis of the structural performance of AM components built by fused filament fabrication

Narges Dialami · Michele Chiumenti · Miguel Cervera · Riccardo Rossi · Uxue Chasco · Miquel Domingo

Received: 11 July 2020 / Accepted: 26 September 2020

Abstract This work analyses the performance of parts built by Additive Manufacturing (AM) using fused filament fabrication (FFF) demonstrating the correlation between the printing orientation and structural performance. FFF components present two regions showing different mechanical behaviour: the external contour and the inner structure (in-fills or lattice). The respective mechanical properties of the contour and the inner structure are obtained. In this work the inner structure is replaced by an anisotropic homogenized material. A Representative Volume Element with Periodic Boundary conditions is adopted to obtain the corresponding equivalent constitutive tensor. On the other hand, the contour is considered isotropic. The material characterization of both the in-fill and the contour is done following two complementary strategies: (1) an experimental campaign involving several tensile tests on FFF specimens; (2) a sensitivity analysis through numerical modelling. Performing experiments to obtain the material properties for contour and in-fill may be a challenging task. Thus, the numerical modelling and the optimization technique are used to obtain the material properties as a function of the filament properties. Calibration of the structural response of 3D-printed demonstrators under bending and torsion is done in order to optimize the material parameters of the numerical model by minimising the difference between the experimental and numerically computed structural stiffness. It is shown that assuming isotropic behaviour for the contour results in a negligible error. The AM software so calibrated can be used for analysing the mechanical performance of FFF components and selecting the optimal printing orientation as well as the contour thickness and in-fill density to satisfy the structural performance required.

Keywords Additive manufacturing · Fused filament fabrication · Representative volume element · Homogenization · Anisotropy

N. Dialami (✉) · M. Chiumenti · M. Cervera · R. Rossi · U. Chasco
International Center for Numerical Methods in Engineering (CIMNE), Universidad Politécnica de Cataluña, Campus Norte UPC, 08034 Barcelona, Spain
e-mail: Narges@cimne.upc.edu

M. Chiumenti
e-mail: Michele@cimne.upc.edu

M. Cervera
e-mail: Miguel.Cervera@upc.edu

R. Rossi
e-mail: Rrossi@cimne.upc.edu

U. Chasco
e-mail: Uxuech9@gmail.com

M. Domingo
Fundació Eurecat, Av. Universitat Autònoma, 23, 08290 Cerdanyola del Vallès, Spain
e-mail: Miquel.Domingo@eurecat.org

Published online: 15 October 2020

1 Introduction

Additive Manufacturing (AM), also known as 3D printing is a technique to fabricate parts and components from a Computer-Aided Design (CAD) model. This is done through layer-by-layer deposition of different materials ranging from polymers to metals, as well as cement-based compounds. The interest in AM technology grows in both the industrial and the scientific communities due to the fabrication versatility it provides, compared to traditional manufacturing technologies. AM has a particularly strong advantage in terms of its capacity of creating complex geometries with cavities or lattice structures. Moreover, AM reduces the assembly time, as it allows part consolidation. These characteristics make AM a powerful cost-effective technology allowing for higher design freedom and customization compared to manufacturing methods such as forging or casting (Attaran 2017; Gibson et al. 2010).

Polymer-based 3D-printing is evolving fast, moving the focus from rapid-prototyping to the fabrication of structural components with enhanced thermal resistance as well as mechanical strength while reducing weight and material use (Guo and Leu 2013). Acrylonitrile butadiene styrene (ABS), polycarbonate (PC) and polylactic acid (PLA) are some examples of polymer-based materials commonly used in AM processes (Ngo et al. 2018).

There are different types of AM techniques where polymer-based materials are commonly used: *Selective Laser Sintering* (SLS) (Yang et al. 2018; Olakanmi et al. 2015); *Multi Jet Fusion* (MJF) (O'Connor et al. 2018; Sillani et al. 2019) and *Fused filament fabrication* (FFF), also known as *Fused Deposition Modelling* (FDM) (Peterson 2019; Brenken et al. 2018).[1]

Generally in AM, the material properties of the final printed component do not coincide with the ones of the raw material (Kotlinski 2014). This occurs due to the layer-by-layer fabrication, characteristic of the AM processes. Moreover, the mechanical performance depends on the resulting microstructure, which is influenced by the local temperature gradients aligned with the building direction.

While some AM types such as SLS or MJF maintain the isotropy of the raw material, in components printed via FFF anisotropic behaviour is observed. Despite the fact that the underlying filament material is isotropic, the anisotropy of a FFF-printed part manifests due to: the layer-to-layer adhesion, the filament-to-filament adhesion and the printing patterns.

The significant material anisotropy and heterogeneity encountered in FFF parts cannot be ignored as it has a significant impact on the mechanical performance of the component (Gray and Baird 2002). This is the reason why establishing a methodology for the material characterization of components fabricated by FFF technology is one of the main focus of the present work.

In FFF, the objects are printed by melting a thermoplastic filament to be extruded through a nozzle. The printing process and, consequently, the final structural behaviour are characterized by different process parameters, the most important ones being the object orientation, the layer thickness and the scanning patterns.

These parameters are defined by the user prior to the slicing of the CAD model. Selecting the optimal process parameters in FFF is critical as this directly affects: (1) the mechanical behaviour of the component (Bellini and Güçeri 2003), (2) its surface texture (Townsend et al. 2016) and, (3) the fabrication cost (Atzeni and Salmi 2012).

The printing patterns can be classified into contour and raster trajectories. The contours define the exterior surface of the 3D object, while both the raster and the in-fill density characterize the inner section bounded by the contour. There are two types of inner structures: the *in-fill* structures and the *lattice* structures (Fig. 1). The in-fill is the standard structure adopted in FFF technology and its density is defined by the raster to raster air gap. The in-fill pattern is repeated for each layer following the printing (vertical) direction. The lattice structures are characterized by a *unit cell* periodically repeated in space. Both structures are used to save material, printing time and production costs.

Figure 2 shows a geometry fabricated with the same printing parameters. Nevertheless, when the loading is aligned with the filament direction (Fig. 2a) the part shows higher stiffness and strength than when loading is applied orthogonal to the printing plane

[1] D. Technology, Materialise fused deposition modeling. https://www.materialise.com/en/manufacturing/3d-printing technology/fused-deposition-modeling.

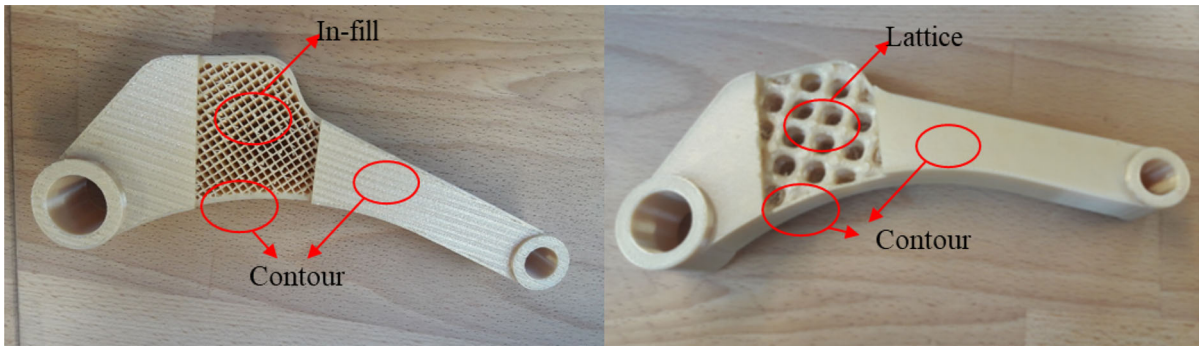

Fig. 1 Types of inner structure: in-fill (left), lattice (right)

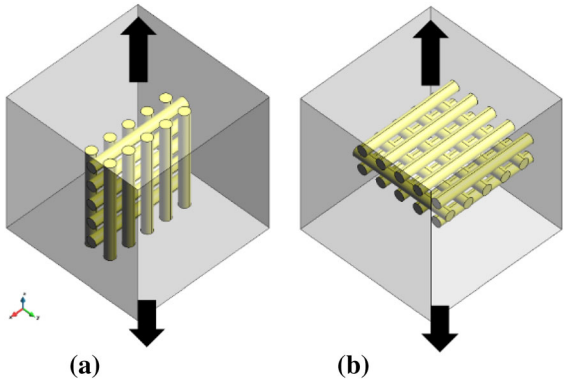

Fig. 2 Filaments pattern depending on the printing orientation: **a** Printing orientation parallel to the loading force; **b** Printing orientation perpendicular to the loading force

(Fig. 2b). Therefore, in case of tensile stresses, the mechanical performance of FFF components improves when the filaments are aligned with the loading (Sood et al. 2010).

Contrariwise under compression it is preferable to align the loading with the stacking direction to avoid buckling (Fig. 3a). However, increasing the compression, sliding between layers due to shear forces can affect the structural integrity (Fig. 3b).

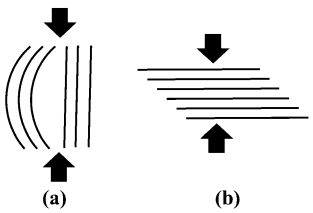

Fig. 3 Scheme of the compressive loading application **a** buckling, **b** shearing

Numerous experiments have reported the strong impact of the component orientation and the raster angle on the properties of the printed parts (Bellini and Güçeri 2003; Domingo-Espin et al. 2015; Thrimurthulu et al. 2004; Delfs et al. 2016; McLouth et al. 2017; Durgun and Ertan 2014; Ziemian et al. 2016; Cantrell et al. 2017; Zaldivar et al. 2017). However, only a few studies are devoted to the numerical simulation of the mechanical performance of FFF builds. Casavola et al. (2016) characterized the orthotropic properties of the FFF parts printed by ABS and PLA utilizing Classical Lamination Theory (CLT). Garg and Bhattacharya (2017) simulated the deformation of the FFF samples under uniaxial loading adopting different raster thicknesses and printing directions. In the majority of the numerical simulation studies, including the above-mentioned ones, FFF components are modelled as a single solid material. However, structural response of contours and inner structures is different, depending on the corresponding building pattern and in-fill density.

In this work, we propose a methodology for characterizing the mechanical performance of components manufactured by FFF technology. This methodology relies on accounting for the mechanical properties of the contours and the inner structures, separately. Both an experimental campaign and a material properties calibration through numerical modelling are carried out. The corresponding mechanical properties of the contour and the in-fill are acquired.

On the experimental side, several dog-bone specimens are manufactured to perform the uniaxial tensile tests in order to characterize the anisotropic behaviour of the printed material. Next, a door-handle

component is fabricated and tested under bending and torsion loading to investigate the influence of the printing orientation, the layer thickness and the in-fill parameters on the actual structural performance. The measured values of both the stiffness and strength shown by these demonstrators are used for the calibration of the numerical model.

On the numerical side, a homogenization technique using the Representative Volume Element (RVE) is used to characterize the inner (lattice and in-fill) structures. The equivalent anisotropic material behaviour is considered for the inner structures while the contour is assumed to be isotropic.

Carrying out experimental tests to determine the material properties for contour and in-fill may be a challenging task. However, the numerical modelling and optimization technique provide an alternative mean for the material characterization. Therefore, an in-house FE software platform is customized to enhance the design of structural components built by FFF.

The outline of the paper is the following: first, the experimental set-up used in this work is presented in Sect. 2. This includes the experimental campaign on different specimens. In Sect. 3, the numerical strategy for material characterization is described. This includes: the constitutive model (Sect. 3.2), the homogenization technique to characterize the in-fill structures (Sects. 3.3 and 3.4) and the sensitivity analysis performed to calibrate the AM model (Sect. 3.5). Finally, in Sect. 4, the results are discussed and future research lines stemming out of the present work are presented.

2 Experimental procedure

This Section describes the experimental procedure carried out for the characterization of the printed material, as well as the tests performed on the demonstrators. The former ones are to analyse the mechanical behaviour of the samples with printing patterns of the external contour. The latter ones are used for the calibration of the numerical model developed and to analyse the mechanical behaviour of a complex structure under different loading conditions.

All the specimens and the demonstrators analysed in the present work were printed and tested by EURECAT *Centre Tecnològic de Catalunya*. The Original Prusa i3 MK2S is the FFF printer used for the manufacturing. *Ultimaker Cura*® is the slicing software used to define the printing parameters of the parts.[2] The printing material is PLA extruded at 215 °C. Linear in-fill (at 45°) is chosen for all the specimens. Table 1 summarizes the printer information.

Table 1 Printer information

Tester	EURECAT
3D printer	Original Prusa i3 MK2S
Printer technology	FFF
Software	Ultimaker Cura
Material	PLA
Extrusion T emp.	215 °C
Type of in-fill	Rectilinear

2.1 Material characterization by experiments

As motivated in the introduction, in this work, the structural behaviour of the external contours and inner structures (in-fill and lattice) are distinguished. For the contour, there exist two main printing patterns used in FFF: (1) aligned filaments and, (2) $\pm$ 45° crossed patterns. The former is used for most of the surfaces when their slope with respect to the printing plane (XY) is greater than 30°. The latter is typically used for the top and bottom covers where the surfaces are almost horizontal (slope less than 30°).

The objective of the experimental work is to compare the material properties of the raw material (filament) with the behaviour of FFF-printed specimens using the above mentioned printing patterns.

On the one hand, the single filament (PLA) is homogeneous and isotropic, and the corresponding elastic parameters are: Young's modulus = 3368 MPa and Poisson's ratio = 0.35 (Tymrak et al. 2014).

On the other hand, dog-bone specimens are printed directly from the CAD model (see Fig. 4) and the corresponding material behaviour is assumed to be orthotropic and aligned with the material directions of the selected printing pattern. Therefore, to fully determine the orthotropic stiffness matrix, nine

[2] Ultimaker. https://ultimaker.com/software/ultimaker-cura.

constants must be calculated: three Young's moduli, three Poisson's coefficients and three shear moduli according to the three directions X, Y and Z. In order to obtain these 9 independent parameters, several specimens are printed in 6 different orientations and tested (uniaxial tensile tests) according to the Standard Test Method for Tensile Properties of Plastics (ASTMD638) (see Figs. 5–10). The cube in Figs. 5, 7 and 9 is shown only for the sake of visualizing the 6 printing orientations.

According to Hooke's law of elasticity, the uniaxial tensile test of a specimen printed according to the orientation 1, defines the Young's modulus in direction X and the Poisson's ratio in XY plane as:

$$E_x = \frac{\sigma_{xx}}{\varepsilon_{xx}}, \quad v_{xy} = -\frac{\varepsilon_{yy}}{\varepsilon_{xx}} \tag{1}$$

Similarly, from orientation 2, one obtains:

$$E_y = \frac{\sigma_{yy}}{\varepsilon_{yy}}, \quad v_{yz} = -\frac{\varepsilon_{zz}}{\varepsilon_{yy}} \tag{2}$$

and from orientation 3:

$$E_z = \frac{\sigma_{zz}}{\varepsilon_{zz}}, \quad v_{xz} = -\frac{\varepsilon_{zz}}{\varepsilon_{xx}} \tag{3}$$

Young's modulus and Poisson's ratio can be obtained by a stress/elongation test with Eqs. 1–3 relating the direction of application of the force or displacement to the one perpendicular to it.

From orientations 4, 5 and 6, the shear moduli are obtained by uniaxial tensile tests of specimens printed at 45° and belonging to the corresponding XY, XZ and YZ printing planes. Thus, the following relationships are used to obtain the shear modulus within each plane (Bellini and Güçeri 2003; Domingo-Espin et al. 2015):

$$G_{xy} = \left.\frac{E_1}{2(1+v_{12})}\right|_{xy} G_{xz} = \left.\frac{E_1}{2(1+v_{12})}\right|_{xz} G_{yz} = \left.\frac{E_1}{2(1+v_{12})}\right|_{yz} \tag{4}$$

where in this case, 1 stands for the direction of the applied load and 2 is the direction perpendicular to 1.

Considering the above, 3 different families of FFF-printed specimens are printed and tested:

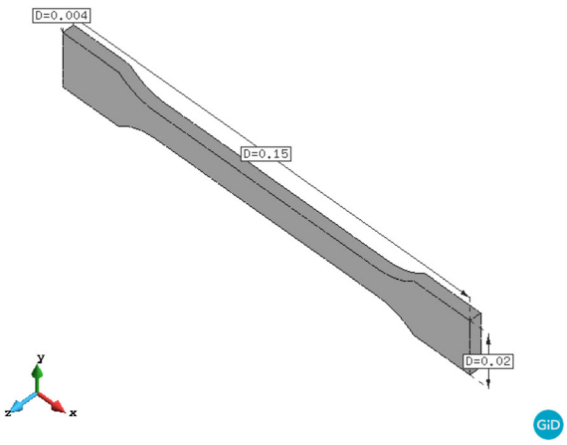

Fig. 4 Geometry of the dog-bone specimens

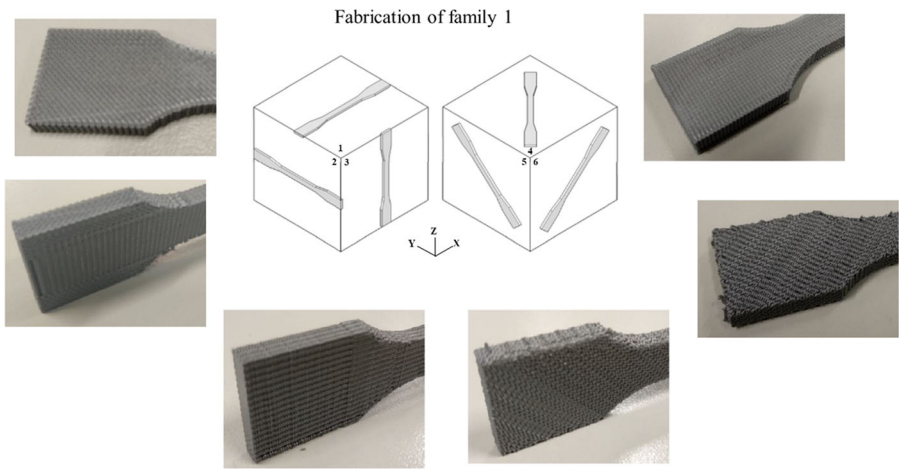

Fig. 5 Crossed-type: 6 printing orientations

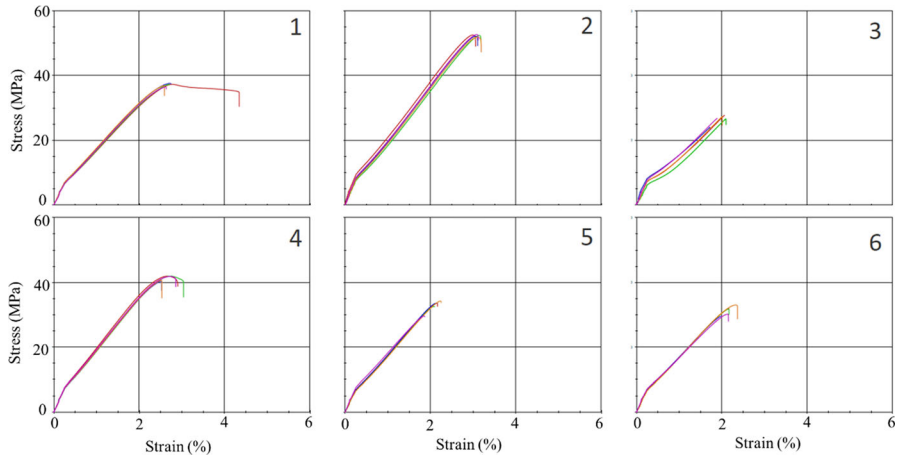

Fig. 6 Stress-strain curves of crossed printing pattern

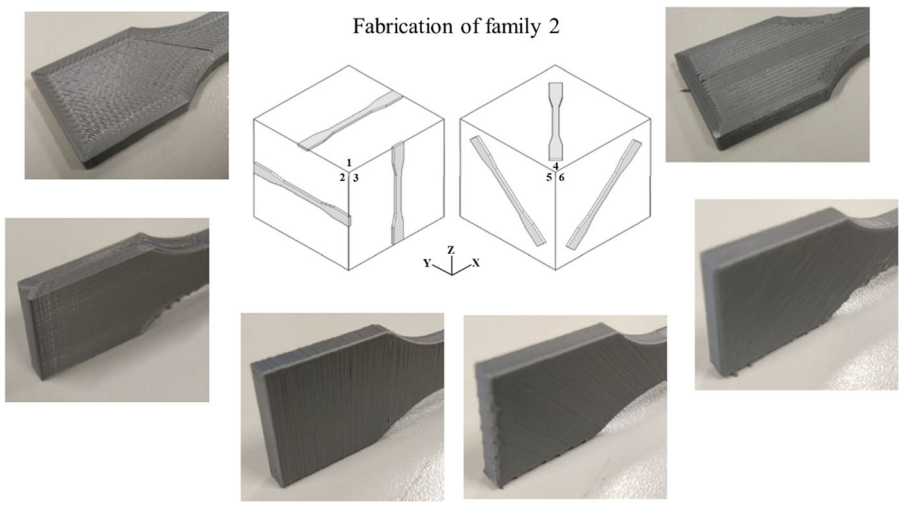

Fig. 7 Mixed-type: 6 printing orientations

1. *Crossed-type*: 30 specimens (5 for each orientation) characterized by ± 45° crossed printing pattern (see Fig. 5).
2. *Mixed-type*: 30 specimens (5 for each orientation) characterized by 5 aligned filaments following the external contour of the dog-bone shape. The rest of the volume is filled by by ± 45° crossed printing pattern (see Fig. 7).
3. *Aligned-type*: 30 specimens (5 for each orientation). In this case, 5 aligned filaments following the external contour are printed, only. Each filament is 0.4 mm tick (see Fig. 9).

Figure 11 shows the printing patterns for the families manufactured in orientation 1. Table 2 summarises the printing patterns of each family. The samples are printed and tested according to the ISO 527-2 1A.

The stress/strain curves obtained for the 3 families and the 6 printing orientations are shown in Figs. 6, 8 and 10, respectively.

The corresponding mechanical properties are presented in Table 3. E_x and v_{xy} are obtained from specimens printed and tested in plane 1 (Plane XY). The aligned-type specimens of orientations 1 and 4 could not be experimentally tested because they have no interior and the tests fail.

Note that the ratio between aligned and crossed pattern of the mixed-type specimens depends on their actual orientation. In particular, only orientations 1 and 4 present mixed printing patterns while for orientations 2, 3, 5 and 6 the aligned filaments occupy

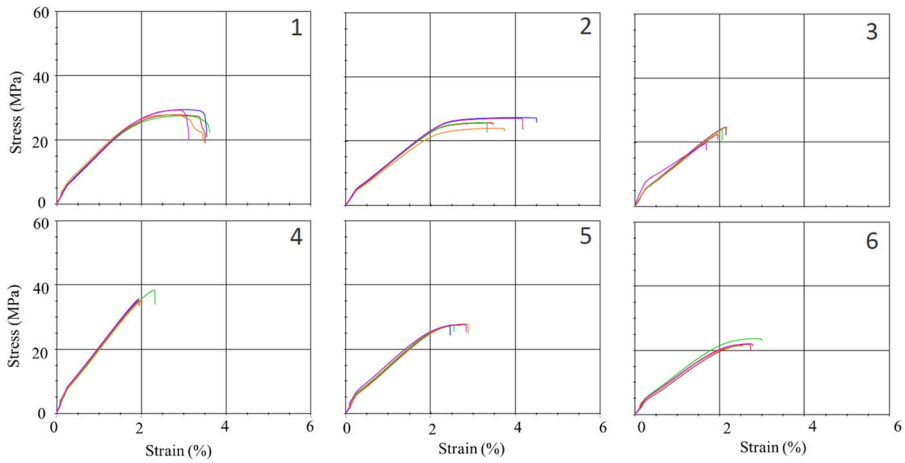

Fig. 8 Stress-strain curves of mixed printing pattern

Table 2 Printing patterns of each family

Family	Pattern
1	Crossed
2	Mixed
3	Aligned

the whole thickness of the dog-bone specimens. Therefore, the elastic constants obtained using these orientations are all equal for families 2 and 3.

This experimental work shows that the mechanical properties of FFF-printed specimens depend on the actual printing pattern. The mechanical behaviour of the aligned-type and crossed-type samples are transversely isotropic. Depending on the printing pattern, the isotropic plane varies. The crossed-type samples are transversely isotropic where XZ is the isotropic plane being the lower stiffness in Y direction. The mixed-type and aligned-type samples are also transversely isotropic. However, YZ is the isotropic plane and the stiffness is lower in X direction. Moreover, it can be concluded that:

(1) The highest stiffness is achieved when the specimens are fabricated with aligned filaments. Nevertheless, the Young's modulus is around 10–15% lower than for the raw material (single filament).

(2) In the case of crossed-type specimens, the material stiffness shows values 30–35% lower than that of the raw material. It must be also noted that the lack of a smooth external contour

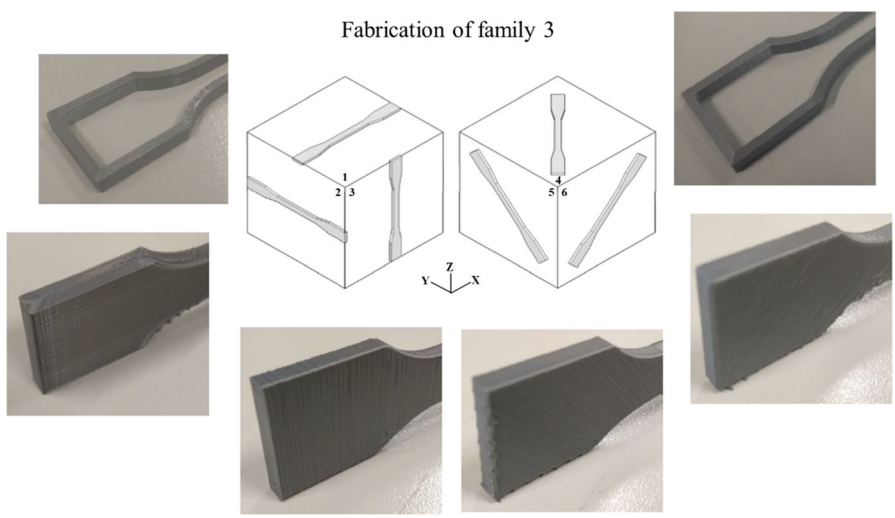

Fig. 9 Aligned-type: 6 printing orientations

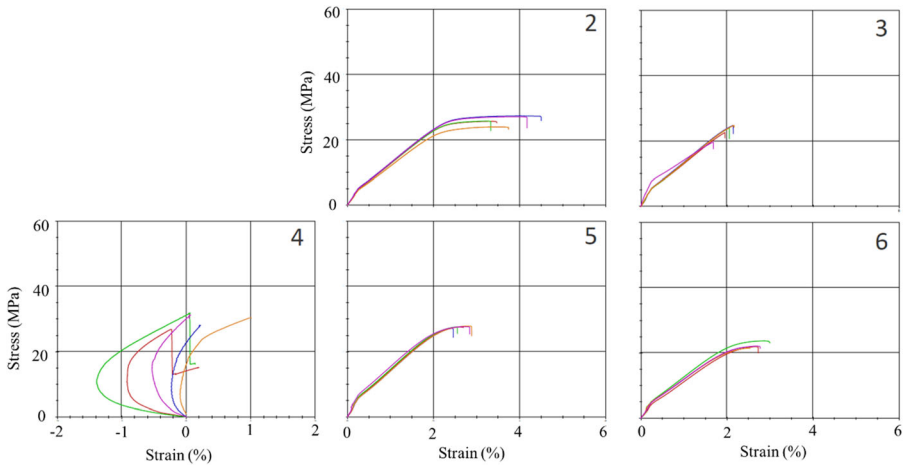

Fig. 10 Stress-strain curves of aligned printing pattern

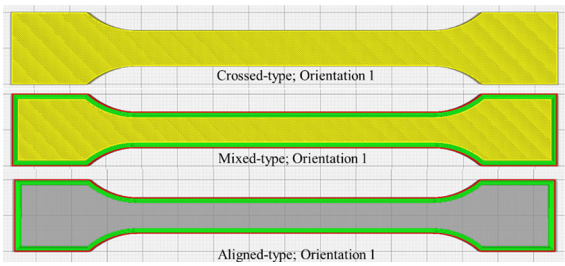

Fig. 11 Crossed, mixed and aligned printing patterns in orientation 1: contour(green) and in-fill (yellow). (Color figure online)

covering the external skin of the specimens generates stress concentration points where cracking can occur.

(3) Some of the orientations are extremely difficult to be tested (e.g. orientations 1 and 4 in Fig. 10).

3 Numerical strategy

In this Section a numerical strategy for predicting the structural performance of components fabricated by FFF is presented. The model is initially fed with the material parameters obtained from the experimental work realized on the dog-bone specimens. Next, these parameters are calibrated through a sensitivity analysis to accurately capture the mechanical response of a demonstrator fabricated in 3 different orientations.

3.1 Mechanical analysis of FFF pieces

In the structural components fabricated by FFF shown in Fig. 1, two regions are distinguished: the external contours and the inner part: either lattice or in-fill structures. Focussing on the external contours, the experimental work carried out demonstrates that: (1) the as-printed material is characterized by a lower material stiffness and strength if compared to the raw material; (2) the external contour can be assumed as transversally isotropic; (3) the printing pattern plays an important role on the material characterization and in the definition of the orientation of both the isotropic plane and the weakest direction.

When modelling industrial components defined by complex geometries, the actual orientation of the

Table 3 Mechanical properties obtained from the tensile test, values are in GPa

Pattern	E_x	E_y	E_z	ν_{xy}	ν_{yz}	ν_{xz}	G_{xy}	G_{yz}	G_{xz}
Crossed	2.464	1.984	2.324	0.259	0.188	0.236	0.332	0.362	0.363
Mixed	2.772	3.171	3.058	0.227	0.221	0.181	0.363	0.340	0.341
Aligned	–	3.171	3.058	–	0.221	0.181	–	0.340	0.341

anisotropy planes of the printed material becomes a challenging task due to the alignment of the filaments with the external surface contour. Moreover, it is not always easy to split this contour by different printing patterns. Thus, the anisotropy of the external surface of a structural component fabricated by FFF cannot be characterized by a unique material reference system. This is the reason why it is reasonable to assume a *homogenised isotropic* behaviour for the numerical model of the external contour. The *mixed-type* material parameters obtained from Family-2 are used as the starting values for the numerical modelling.

The most standard inner structure in FFF is characterized by an alternating sequence of + 45° and − 45° rasters piled up in the building (vertical) direction, being the in-fill density, a printing parameter defining the raster-to-raster spacing.

The in-fill structure is heterogeneous and its discretization by the standard FE mesh would result in an excessive number of elements, precluding efficient numerical computations. Alternatively, it can be modelled as an *equivalent* homogeneous continuum taking advantage of its repetitive cell structure. Hence, in the present work, a homogenization method is adopted to characterise the corresponding *anisotropic* elastic behaviour.

3.2 Constitutive modelling of the 3D-printed components

The aim of this work is to perform characterization of the structural *stiffness* of AM components built by FFF. The constitutive behaviour will be characterized by a linear elastic model:

$$\boldsymbol{\sigma}_m = \boldsymbol{C}_m : \boldsymbol{\varepsilon}_m \tag{5}$$

where $\boldsymbol{\sigma}_m$ and $\boldsymbol{\varepsilon}_m$ are the Cauchy stress and strain tensors, respectively. $\boldsymbol{C}_m$ is the constitutive (stiffness) tensor of the material. Alternatively, the constitutive relationship can be written as:

$$\boldsymbol{\varepsilon}_m = \boldsymbol{D}_m : \boldsymbol{\sigma}_m \tag{6}$$

where $\boldsymbol{D}_m = \boldsymbol{C}_m^{-1}$ is the compliance (flexibility) tensor, defined as the inverse of the stiffness tensor.

The *transversely isotropic* constitutive model is suitable for the *inner structures* and, particularly, for the *in-fill structures* fabricated by FFF technology. Its use is justified thanks to the periodic arrangement of the unit cells and the printing evolution in the building direction. Being XY the symmetry plane (built plate) and Z, the building direction, the flexibility tensor of transversely isotropic materials is defined by 5 independent parameters: $E = E_x = E_y$, E_z, ν_{xy}, ν_{zx}, $G = G_{zx} = G_{yz}$:

$$\begin{bmatrix} \frac{1}{E} & -\frac{v_{xy}}{E} & -\frac{v_{zx}}{E_z} & 0 & 0 & 0 \\ -\frac{v_{xy}}{E} & \frac{1}{E} & -\frac{v_{zx}}{E_z} & 0 & 0 & 0 \\ -\frac{v_{zx}}{E_z} & -\frac{v_{zx}}{E_z} & \frac{1}{E_z} & 0 & 0 & 0 \\ 0 & 0 & 0 & \frac{2(1+v_{xy})}{E} & 0 & 0 \\ 0 & 0 & 0 & 0 & \frac{1}{G} & 0 \\ 0 & 0 & 0 & 0 & 0 & \frac{1}{G} \end{bmatrix}, \tag{7}$$

where E_i is the Young's modulus along axis i, G_{ij} is the shear modulus in direction j on the plane whose normal is in direction i, and finally, v_{ij} is the Poisson's ratio defining the relationship between the transversal deformation (direction j) and the axial elongation (when the loading is applied in direction i).

The *contour structures* are modelled as an *isotropic* material behaviour, characterized by:

$$\begin{bmatrix} \frac{1}{E} & -\frac{v}{E} & -\frac{v}{E} & 0 & 0 & 0 \\ -\frac{v}{E} & \frac{1}{E} & -\frac{v}{E} & 0 & 0 & 0 \\ -\frac{v}{E} & -\frac{v}{E} & \frac{1}{E} & 0 & 0 & 0 \\ 0 & 0 & 0 & \frac{2(1+v)}{E} & 0 & 0 \\ 0 & 0 & 0 & 0 & \frac{2(1+v)}{E} & 0 \\ 0 & 0 & 0 & 0 & 0 & \frac{2(1+v)}{E} \end{bmatrix}, \tag{8}$$

The compliance tensor of isotropic materials depends on 2 independent parameters only, the Young's modulus and the Poisson's ratio.

3.3 The representative volume element

Standard FE analysis of AM parts with inner structures such as in-fill or lattice structures is challenging because of the complexity of generating FE meshes suitable for such complex geometries. Generally, the FE discretization of in-fill structures as the one shown in Fig. 1 implies a prohibitively high computational cost.

Let us consider two different scales of analysis: the global (macro) scale corresponding to the AM component and the local (micro) scale characterizing the inner structure accounting for both material and geometrical heterogeneities.

There are 3 main approaches to model heterogeneous structures:

1. The first approach is the *Direct Numerical Simulation* (DNS) where standard FE analysis is used, and all the information about the micro-structure is explicitly modelled (Lourenço and Rots 1997). This approach is efficient for small-scale analysis, but it soon becomes unaffordable for industrial studies because of the huge computational requirements in terms of both memory and CPU-time.
2. The second approach is known as *Concurrent Multiscale Method* (CMM), where a multiscale analysis involving the study of both length scales and the corresponding exchange of information among them is used. The micro-scale is solved at each sampling point of the structural model (macro-scale), establishing a strong coupling between macro and micro scales (Lloberas-Valls et al. 2011, 2012). This method is also known as FE^2 method because FE analysis is required at both scales.
3. The third approach is the *Computational Homogenization Method* (CHM). This approach establishes a weak coupling assuming a separation between the two length scales (Nguyen et al. 2011). Therefore, the heterogeneities of the micro-scale are not directly inserted into the structural analysis but modelled through the definition of a *Representative Volume Element* (RVE). The RVE is then used to extract a structurally equivalent, homogeneous and generally anisotropic, constitutive behaviour to feed the macroscale at component level (Oller et al. 2005; Otero et al. 2012, 2015).

In this work, the homogenization strategy is adopted to replace the complex inner structure by a continuum (homogenous) one, characterized by an equivalent structural response. This is feasible because of the *periodicity* of both in-fill and lattice structures defined by the repetition of a *unit cell*. Therefore, at global (component) level the volume is assumed to be anisotropic but homogeneous, while the heterogeneous internal geometry of in-fill or lattice structures is represented in the RVE (see Fig. 12). Note that the main hypothesis defining the accuracy of the mechanical response of the RVE is based on the actual *scale separation*. Thus, the size of the printed part must be much larger than the RVE adopted for the homogenization procedure (Hill 1963).

3.4 Homogeneization procedure

First-order homogenization is used in this work, where the strains are used as the link between the macro (component level) and the micro (inner structure) scales.

The problem at the microscale (RVE) is solved considering especial boundary conditions and then the homogenized variables are calculated through averaging equations (Suquet 1985).

The homogenization procedure consists of the following steps:

1. *Down-scaling*. The information is passed from the global (macro) scale to the local (micro) scale defined in terms of the RVE. Hence, the macroscopic strains, computed at the sampling points of the computational mesh used to discretize the AM component, are transferred to the RVE. According to the first-order homogenization technique, a *linear* displacement field is defined at each point $\boldsymbol{X}$ in the macro-scale. Therefore, the macroscopic strains $\boldsymbol{\varepsilon}_m(\boldsymbol{X})$ are *constant*. On the other hand, the displacement field at each point $\boldsymbol{x}$ of the micro-scale (RVE) is much richer and cannot be solved by the coarse FE mesh used at the global level. The computational homogenization method assumes that the macroscopic strains are obtained as the volume average of the microscopic strains, $\boldsymbol{\varepsilon}_\mu(\boldsymbol{x})$ as:

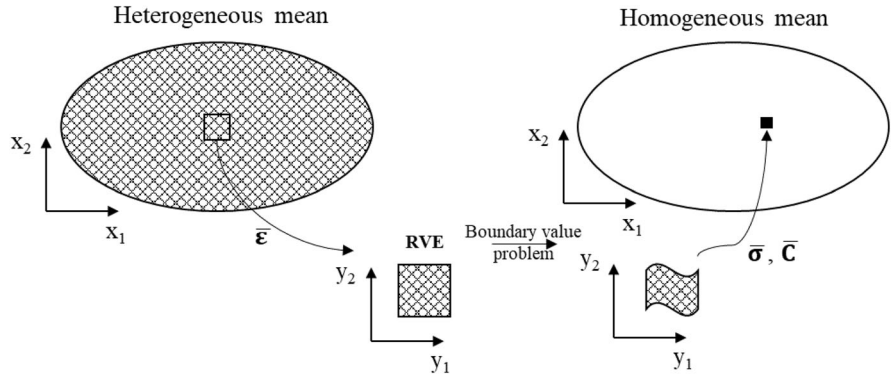

Fig. 12 Homogenization strategy

$$\boldsymbol{\varepsilon}_m(\boldsymbol{X}) = \frac{1}{V_{RVE}} \int_{V_{RVE}} \boldsymbol{\varepsilon}_\mu(\boldsymbol{x}) dV \tag{9}$$

2. *Solution of the RVE problem.* Applying the Principle of Virtual Work, a Boundary Value Problem (BVP) defines the equilibrium of the RVE as:

$$\int_{V_{RVE}} d\boldsymbol{\varepsilon}_\mu(\boldsymbol{x}) \boldsymbol{\sigma}_\mu(\boldsymbol{x}) \; dV = F \tag{10}$$

where $\boldsymbol{\sigma}_\mu(\boldsymbol{x}) = \boldsymbol{C}_\mu(\boldsymbol{x})\boldsymbol{\varepsilon}_\mu(\boldsymbol{x})$ is the stress field at each point of the computational domain, being $\boldsymbol{C}_\mu(\boldsymbol{x})$ the constitutive tensor. F is the work of the external loads, defined as:

$$F = \int_V \boldsymbol{v}_\mu(\boldsymbol{x}) \boldsymbol{b} dV - \int_V d\boldsymbol{\varepsilon}_\mu(\boldsymbol{x}) \boldsymbol{C}_\mu(\boldsymbol{x}) \boldsymbol{\varepsilon}_m dV \tag{11}$$

being $\boldsymbol{v}_\mu(\boldsymbol{x})$ and $d\boldsymbol{\varepsilon}_\mu(\boldsymbol{x})$ the virtual displacements and the virtual strains, respectively.
Problem (11) must be complemented with the corresponding boundary conditions. In this work, the *Periodic Boundary Conditions* (PBC) are adopted for the solution of the BVP on the RVE:

$$\tilde{\boldsymbol{u}}(\boldsymbol{x}^+) = \tilde{\boldsymbol{u}}(\boldsymbol{x}^-) \quad \forall \{\boldsymbol{x}^+, \boldsymbol{x}^-\} \in \Gamma_{RVE} \tag{12}$$

where $\boldsymbol{x}^+ \in \Gamma^+_{RVE}$ and $\boldsymbol{x}^- \in \Gamma^-_{RVE}$ are *all* pairs of *opposite points* belonging to the RVE boundary $\Gamma_{RVE} = \Gamma^+_{RVE} \cup \Gamma^-_{RVE}$.
This is the natural choice for both the in-fill and the lattice structures because of their actual periodicity. Moreover, their specific *unit cells* are selected as the optimal (most reduced) RVE domains.

3. *Up-scaling.* The solution obtained at local level is returned to the macro-scale through the homogenization process over the RVE. As a consequence of the Hill-Mandel Principle of Macro-Homogeneity (Hill 1965; Mandel 1971), the stresses at the global level are obtained as the volume average of the local stresses computed on the RVE, as:

$$\boldsymbol{\sigma}_m(\boldsymbol{X}) = \frac{1}{V_{RVE}} \int_{V_{RVE}} \boldsymbol{\sigma}_\mu(\boldsymbol{x}) dV \tag{13}$$

The homogenized (*anisotropic*) constitutive tensor, $\boldsymbol{C}_m$, is obtained as:

$$\boldsymbol{C}_m = \boldsymbol{S} \cdot \boldsymbol{E}^{-1} \tag{14}$$

where $\boldsymbol{S}$ is a matrix such that each column corresponds to the vector (Voigt's notation) of global stresses $\boldsymbol{\sigma}_m^{(i)}$, obtained through the homogenization process in Eq. 13, after solving the ith BVP defined by Eq. 10. Thus:

$$\boldsymbol{S} = \left[\boldsymbol{\sigma}_m^{(1)} \quad \cdots \quad \boldsymbol{\sigma}_m^{(6)} \right] = \begin{bmatrix} \sigma_{m,x}^{(1)} & \cdots & \sigma_{m,x}^{(6)} \\ \vdots & \ddots & \vdots \\ \sigma_{m,yz}^{(1)} & \cdots & \sigma_{m,yz}^{(6)} \end{bmatrix} \tag{15}$$

Therefore, each BVP is characterized by a loading condition (3 elongations and 3 distortions) defined in terms of the corresponding prescribed strain field: $\boldsymbol{\varepsilon}_m^{(i)}$, $i = [1, 6]$. Hence, the matrix $\boldsymbol{E}$ is filled with the components of the global strains, $\boldsymbol{\varepsilon}_m^{(i)}$, as:

$$\boldsymbol{E} = \left[\boldsymbol{\varepsilon}_m^{(1)} \quad \cdots \quad \boldsymbol{\varepsilon}_m^{(6)} \right] = \begin{bmatrix} \varepsilon_{m,x}^{(1)} & \cdots & \varepsilon_{m,x}^{(6)} \\ \vdots & \ddots & \vdots \\ \varepsilon_{m,yz}^{(1)} & \cdots & \varepsilon_{m,yz}^{(6)} \end{bmatrix} \tag{16}$$

3.5 Calibration of the numerical model

In this Section a door-handle demonstrator is used for the calibration of the numerical model developed. A sensitivity analysis is carried out to calibrate the material properties of both the in-fill and the contour structures by comparison with the experimental measurements.

The door-handle components are fabricated using the same material (PLA) and the same FFF printer as the ones used for the experimental campaign on dog-bone samples.

The dimensions of the component are illustrated in Fig. 13. Three different orientations are considered in the fabrication as shown in Figs. 14 and 15. The numerical model is also expected to predict the structural performance of FFF components according to the printing orientation chosen.

The supporting structures (breakaway type) shown in blue in Fig. 14 are fabricated using the same material as the component. Such structures are generally required when the external surfaces exhibit an angle lower than 30° with respect to the horizontal (XY) plane.

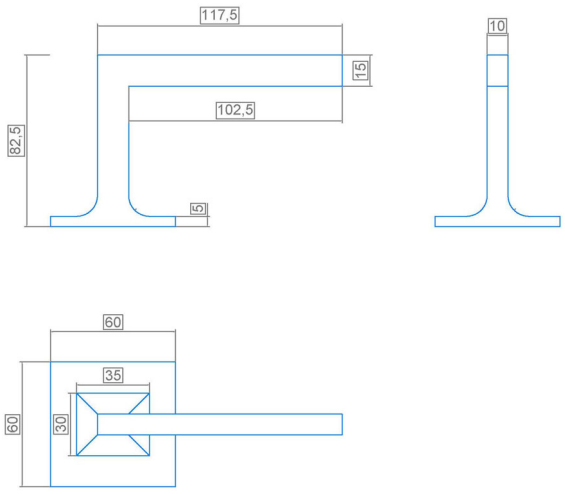

Fig. 13 Dimensions of the door handle tested

The door-handle components are divided into 4 families. Each family is characterized by 2 different in-fill densities (25% and 50%, respectively) and 2 types of contours: single or double contour thickness. Table 4 summarizes the different printing parameters that characterize the 4 families.

The different printing patterns and orientations are generated using the Cura software by Ultimaker. The in-fill is characterized by $+45°/-45°$ alternating raster configuration (Garg and Bhattacharya 2017; Sood et al. 2012).

A cross section of the demonstrator printed in orientation 1 is shown in Fig. 16. Both in-fill densities, as well as, the 2 different contour thicknesses of the external contour can be clearly appreciated.

The loading consists of an imposed vertical displacement of 35 mm applied at 15 mm from the end of the door-handle and applied at a loading speed of 1 mm/min. Thus, a combination of bending and torsion characterizes the resulting stress state as shown in Fig. 17.

The mechanical performance is analysed for each orientation and any combination of the printing parameters under the same loading conditions. The load versus displacement curve is recorded for each test. In this work, only the linear elastic behaviour, characterized by the structural stiffness of the demonstrator is analysed.

The calibration of the mechanical model combines the use of the several software modules. Figure 18 shows the flow chart of the numerical procedure used.

In the present work, a specific KRATOS module (Dadvand et al. 2010) has been implemented to extract the constitutive tensor of the actual in-fill or lattice structure (see Fig. 19). Periodic boundary conditions are applied to the RVE in the homogenization procedure. A sensitivity analysis on the number of unit cells of the original in-fill structure is performed as shown in Fig. 20. It is found out that, adopting periodic boundary conditions, the mechanical response is not sensitive to the number of unit cells. Therefore, the size of the RVE can be reduced to the size of one unit cell minimizing the computational cost.

It must be noted that the anisotropic behaviour of the in-fill (or lattice) structures depends only on the geometrical features that characterize the unit cell. Thus, the same properties of the printed material

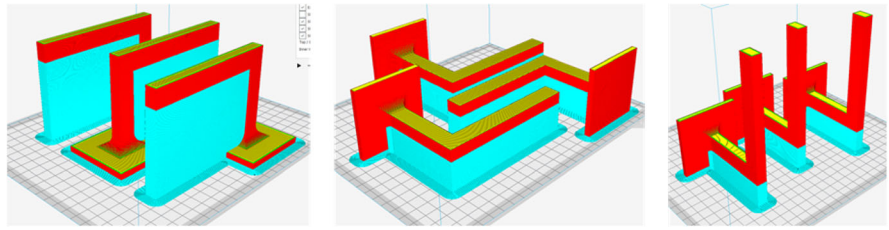

Fig. 14 Door handle demonstrator: orientation 1, 2, 3 (left to right)

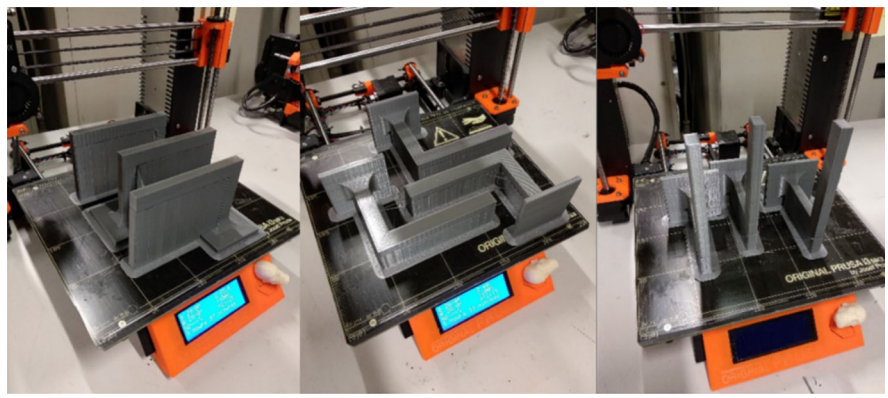

Fig. 15 Door handle samples printed in orientation 1, 2, 3 (left to right)

Table 4 Door handle printing information

In-fill density (%)	50	25
N° filaments × contour	4 (double contour)	2 (single contour)
Printing orientation	3 orientations	
Material	PLA	

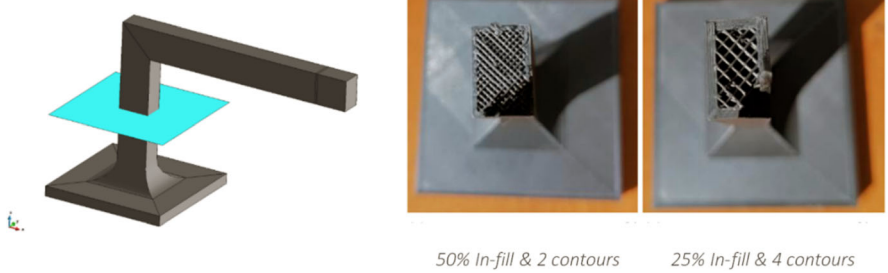

Fig. 16 Door handle printed in orientation 1. Cross section characterized by 50% in-fill and a single contour (left); 25% in-fill and double contour (right)

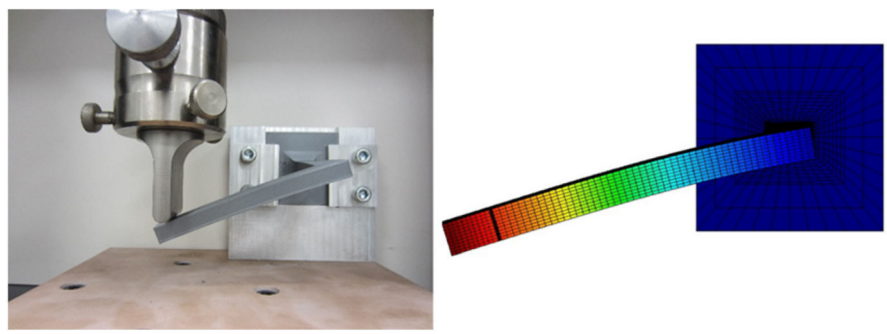

Fig. 17 Experimental set-up and load location (left) Numerical result (right)

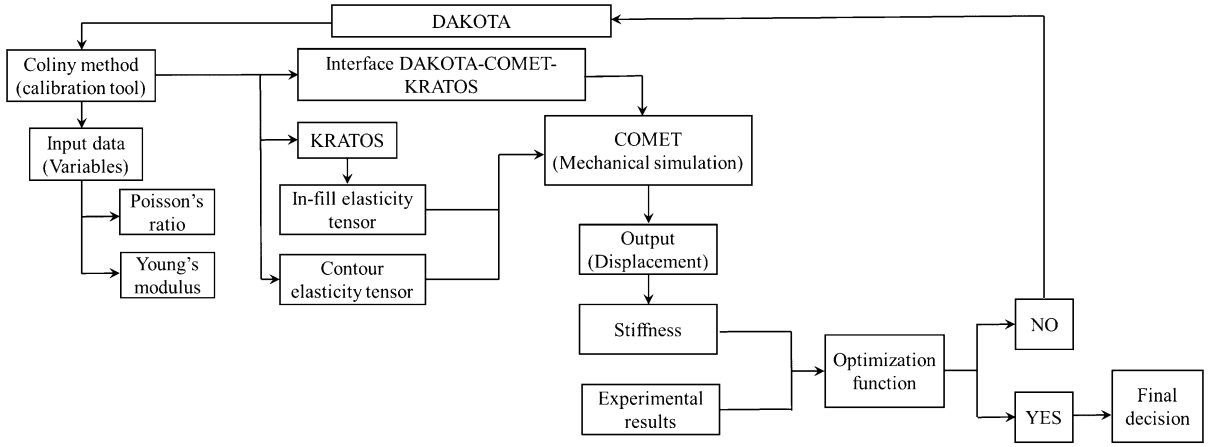

Fig. 18 Flow chart of the iterative process used for the numerical calibration

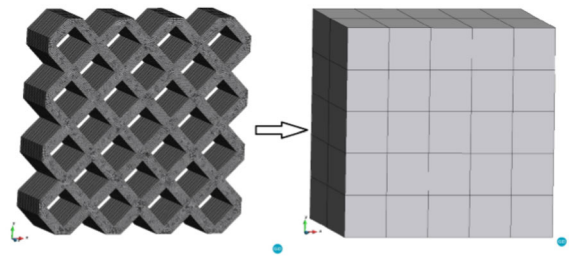

Fig. 19 Homogenization procedure using RVE: from the heterogeneous in-fill structure (left) to the homogeneous but anisotropic counterpart (right)

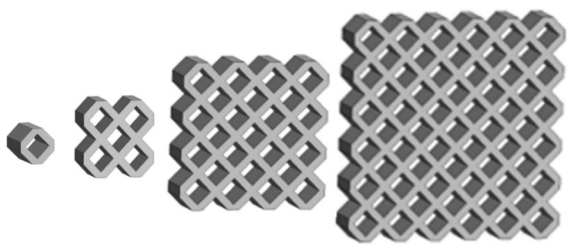

Fig. 20 Several RVE domains used for the sensitivity analysis

adopted for the external contours are used to characterize the bulk material of the in-fill structure.

This homogenization module is used to generate an *off-line* data-base including the most typical in-fill and lattice structures used in FFF.

The overall structural behaviour according to the mechanical loading and boundary conditions applied is computed using COMET, a finite element based in-house software (Cervera et al. 2002).

As discussed before, the volume of the component to be analysed is split into two computational domains: the contour and in-fill structure, respectively. The contour is assumed to be homogeneous and isotropic while the in-fill (or lattice) structure is replaced by the equivalent homogeneous but anisotropic constitutive tensor computed by the KRATOS homogenization module.

In this work, DAKOTA, a well-known open source optimization tool developed by Sandia National Labs (Adams et al. 2013), is used to calibrate the numerical model and, in particular, to minimize the difference between the structural stiffness as experimentally measured, and its numerical counterpart. The procedure is repeated for the 3 orientations and 2 set of printing parameters: (1) single contour (2 filaments) and 50% in-fill; (2) double contour (4 filaments) and 25% in-fill.

The initial guess of the calibration loop is taken from the values of the Young's modulus and the Poisson's ratio as proposed by the filament manufacturer. The admissible range is defined according to the values obtained through the experimental campaign for Family-2. Therefore, the Young's modulus is allowed to vary between 2700 and 3200 MPa and the Poisson's ratio between 0.18 and 0.25. Coliny *derivative-free* method is chosen to find their optimal values minimizing the objective function, S defined as:

$$S = \sum_{i=1}^{n} r_i^2, \tag{17}$$

where $r_i = K_{exp,i} - K_{sim,i}$, are the residual errors between the computed and the experimental values of the structural stiffness, $K_{sim,i}$ and $K_{exp,i}$, respectively. These values are computed as the slope of the load versus displacement curves according to each printing configuration (i), defined in terms of both orientation and process parameters setup.

4 Results

In this section, the mechanical properties obtained through the calibration procedure for both contour and in-fill materials are shown in Tables 5 and 6, respectively.

Comparing these values with the material properties of the raw material, a difference of about 20% in Young's modulus and 30% in the Poisson's ratio is observed. The properties of the raw material result to be stiffer than the ones of the printed components.

Table 7 shows the relative error between the structural stiffness as measured experimentally and by numerical simulation for each printing orientation and set of process parameters. The relative error is below 7% for most of the cases; thus, a good calibration of the demonstrator is achieved.

The load versus displacement curves obtained for all orientations are shown in Figs. 21 and 22 for the cases of 4 filaments and 2 filaments through the contour thickness, respectively. A very good agreement between the numerical simulation and the experimental results is obtained.

As expected, the highest structural stiffness is shown by the family printed with the thickest external contour (4 filaments) and the densest in-fill structure (50%). Contrarily, the most flexible configuration corresponds to 2 filaments through the contour and 25% in-fill. Therefore, it is also possible to conclude that the structural stiffness generally depends on the size of the external contour, while the in-fill has a minor role.

Table 5 Optimized values for the contour

Mechanical properties	Contour
Young's modulus (MPa)	2700
Poisson's ratio	0.25

Table 6 Transversally isotropic properties for the homogenized in-fill

%In-fill		25%	50%
Young's modulus (MPa)	E_x	15.494	179.3
	E_y	15.494	179.24
	E_z	674.96	1350.0
Shear modulus (MPa)	G_{xy}	186.71	393.21
	G_{yz}	150.39	344.97
	G_{xz}	150.39	344.98
Poisson's ratio	ν_{xy}	0.9599	0.8049
	ν_{yz}	0.0057	0.0332
	ν_{xz}	0.0057	0.0332

For each family, orientation 2 is more flexible than the other two orientations, while the orientations 1 and 3 show very similar structural behaviour. Moreover, the numerical results corresponding to this weaker orientation, and particularly when using the lowest in-fill density and contour thickness, exhibits the worst numerical agreement because the original hypothesis of linear elastic response is no longer fulfilled, as clearly shown by the load versus displacement curves (see Fig. 21). Contrarily, for stiffer solutions the relative error reduces to 3.75% (Fig. 23).

From the analysis of the demonstrator, it can be concluded that the strategy adopted for the numerical simulation of structural behaviour of AM components built by FFF is adequate as long as the hypotheses (e.g. linear elasticity, small strains, scales separation for in-fill structure homogenization, etc.…) apply. Moreover, the numerical simulations performed confirmed that modelling the contour of the door handle as isotropic is an acceptable choice.

5 Discussion and future lines

The experimental campaign carried out in this work supports that FFF indices anisotropic behaviour of the built parts, enhancing the relevance of the printing orientation as the most important issue to be considered to optimize the structural behaviour.

Table 7 Best numerical approximation of the mechanical response of the door-handle and the relative error according to each orientation and printing parameters

Orientation	# Filaments	In-fill %	Displacement (mm)	$K_{Numerical}$ (MPa)	Force (N)	$K_{Experimental}$ (MPa)	ε_{rel} %	r_i^2
1	4	25	5.73643	2.615	15	2.4435	7	0.029366793
2			7.44865	2.014		1.8769	7	0.018738037
3			6.16746	2.432		2.5339	4	0.010359478
1	4	50	5.32085	2.819	15	3.0005	6	0.032907137
2			6.46861	2.319		2.4316	5	0.012703
3			5.40936	2.773		3.0127	8	0.057469164
1	2	25	8.50330	1.764	15	1.5999	10	0.026935963
2			11.11501	1.350		1.109	22	0.057852974
3			8.66519	1.731		1.6425	5	0.007843543
1	2	50	7.17343	2.091	15	2.1333	2	0.001785185
2			8.73482	1.717		1.6751	3	0.001777926
3			6.83087	2.196		2.2664	3	0.004968353
							S	0.262707552

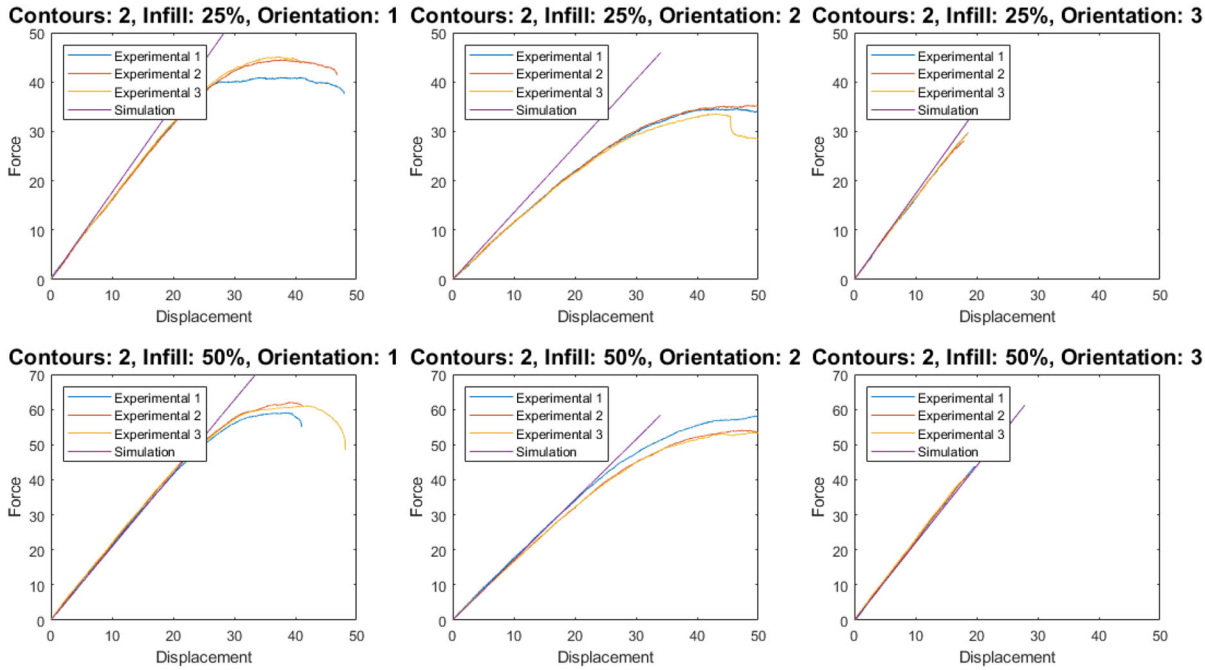

Fig. 21 Force [N] versus displacement [mm] curves comparing the simulation results with the experimental measurements (single contours)

The printing patterns chosen by the most common slicer tools (e.g. Cura, Magic, etc.…) typically vary as a function of the slope of the external contour with respect to the built plane. On the one hand, when the angle between the built plate and the contour is higher than 30°, the filaments are aligned with the contour orientation and piled up according to the layer-by-layer AM strategy. On the other hand, when this angle

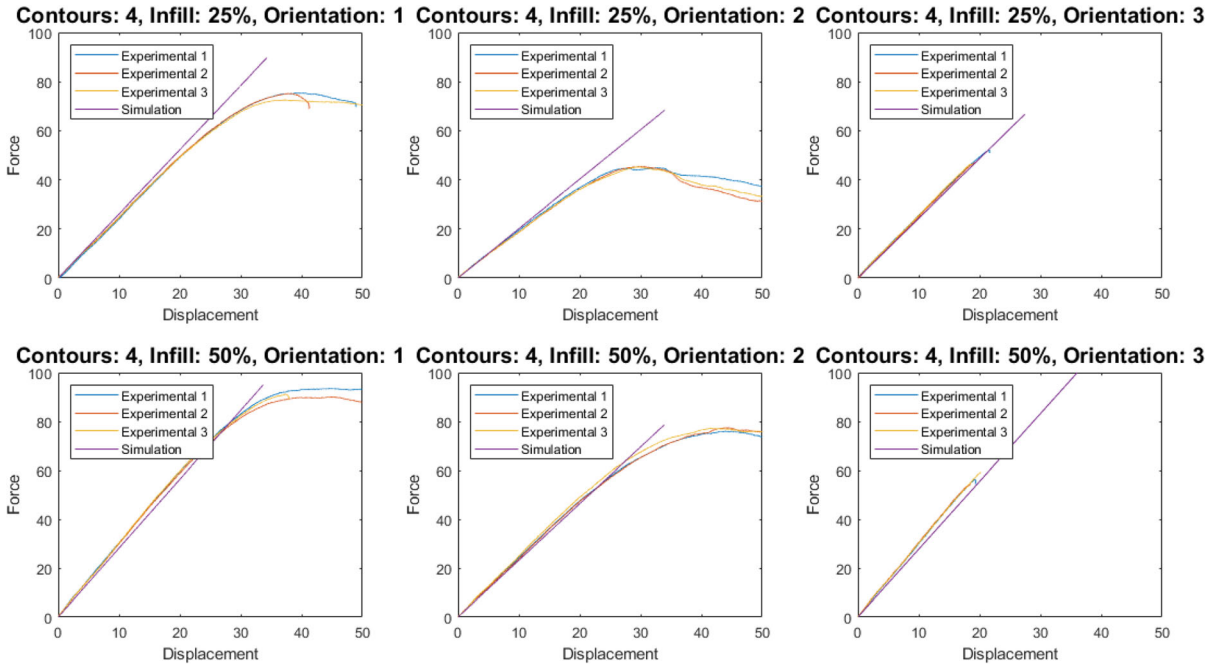

Fig. 22 Force [N] versus displacement [mm] curves comparing the simulation results with the experimental measurements (double contours)

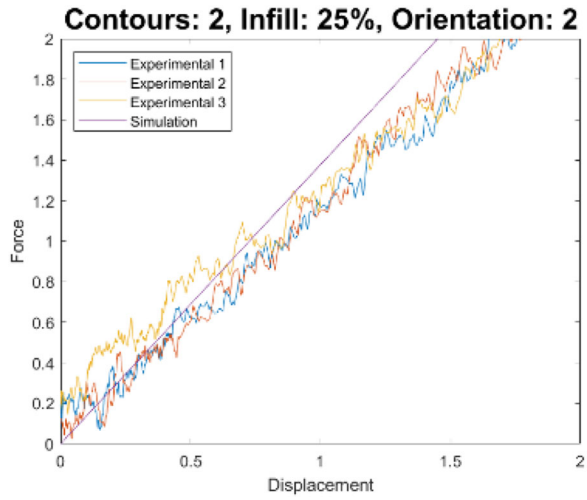

Fig. 23 Force [N] versus displacement [mm] curves for the simulation results and the experimental tests (2 contours and 25% in-fill and orientation 2)

is lower than 30° and, most typically, for horizontal contours (covers, etc.) the crossed + 45°/− 45° patterns is usually preferred. We will refer to the latter as 100% in-fill because the raster distribution is the same as used for the fabrication of the in-fill structures but, in this case, the entire volume is (100%) filled by the extruded material.

Figure 24 shows both contours for each orientation where the yellow and green colours are the 100% in-fill and the contour with aligned filaments, respectively.

The contour surfaces parallel to the printing plane (XY) are made of 100% in-fill with raster distribution, while the contour surfaces growing in the vertical direction (Z) are made of aligned filaments.

Figure 25 illustrates the different parts of the door handle component including in-fill and contours of 100% in-fill and filaments.

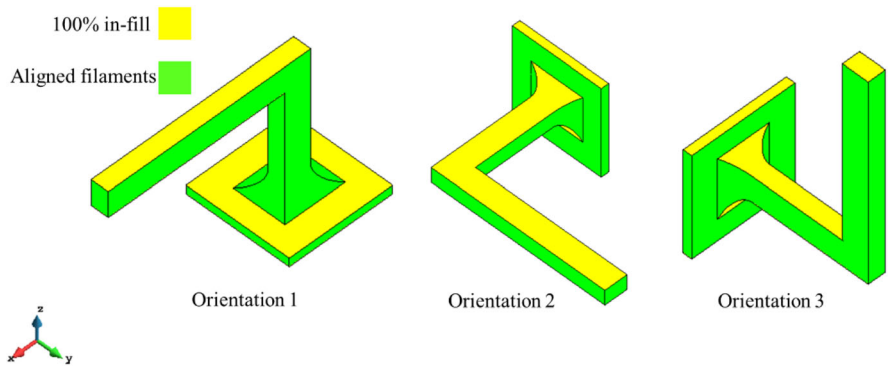

Fig. 24 Three printing orientations considered for the door handle: 100% in-fill contours (yellow); contours with aligned filaments (green). (Color figure online)

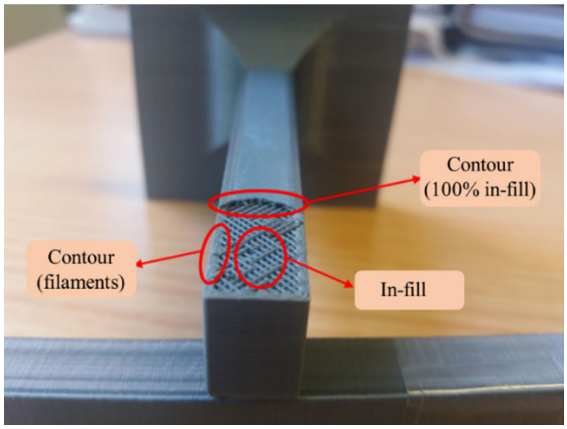

Fig. 25 Different printing patterns of the actual door handle component

Contours printed with aligned filaments present a different mechanical behaviour, in terms of both stiffness and strength, compared to those made by 100% in-fill. This is mostly due to the adhesion among filaments. Thus, adhesion plays a key role in FFF, being the contact surface among filaments related to the selected printing pattern. This supports further investigation of the sensitivity of the mechanical behaviour with respect to the selected printing patterns. An extended experimental campaign is required to perform tensile tests on FFF specimens with different printing patterns used.

6 Summary and conclusions

In this work, the mechanical performance of the AM components made by FFF is analysed experimentally and numerically. The geometry of printed parts is split into two parts: the external contours and the inner structure (in-fill or lattice structures). The material of the external contour surfaces is characterized experimentally by tensile tests on printed dog-bone specimens. It is observed that the material parameters are about 20–30% lower compared to that of the raw material. Moreover, the mechanical behaviour of the aligned-type and crossed-type samples are transversely isotropic. Depending on the printing pattern, the isotropic plane varies. The crossed-type samples are transversely isotropic where XZ is the isotropic plane with the stiffness lower in Y direction. The mixed-type and aligned-type samples are also transversely isotropic. However, YZ is the isotropic plane and the stiffness is lower in X direction.

A homogenization technique is applied to the inner structures to obtain the equivalent homogeneous but anisotropic counterpart to be used for the numerical analysis of both in-fill and lattice structures. Periodic Boundary Conditions (PCB) are applied to the selected RVE to obtain the required constitutive tensor. This strategy is repeated *off-line* to generate a data-base for the most common inner structures identified according to their printing patterns and raster densities.

Different software modules are developed to conform the numerical platform used for the numerical simulation: Kratos, an in-house multi-physics software, is used to characterize the inner structures by RVE homogenization techniques; Comet, another in-house FE solver, is used for the overall structural analysis of AM components. Finally, Dakota, an optimization software, is used as to drive the optimization loop used for the calibration procedure. The optimal material parameters are obtained by minimizing the difference between the numerical results and the experimental measurements.

The door-handle components printed along 3 different orientations and adopting several printing parameters are used as demonstrators. The numerical simulations performed confirmed that modelling the contour of the door handle as isotropic is an acceptable choice.

The good agreement achieved validates the numerical strategy adopted, and, therefore, the predictive capability of the proposed numerical model.

Moreover, the correlation between the printing orientation and the structural performance of FFF components is demonstrated. This shows that it is important to select the optimal printing orientation as well as the most suitable contour thickness and in-fill density to satisfy the structural performance required.

It is also shown that the mechanical properties of the inner structures are much lower compared to the stiffness of the external contour. However, the use of these inner structures improves the structural performance of a FFF part enhancing structural stability of the overall component according to their raster density and printing orientation.

Overall, the relevance of the present work is that it raises the topic of distinguishing between the mechanical behaviour of the contour and the in-fill structures, and the determination of their respective mechanical properties. On the one hand, performing experiments to characterize the contour and the in-fill is a challenging task. On the other hand, it is possible to calibrate the numerical model through a sensitivity analysis based on the as-printed elastic parameters. Moreover, it is shown that assuming an isotropic behaviour for the external contour results in a negligible error.

Acknowledgements This work has been supported by the RIS3CAT Llavor 3D Community co-financed by the Generalitat de Catalunya (ACCIÓ) through the projects TRANSPORT COMRDI16-1-0010 - 00 and PRO2 COMRDI16-1-0009-04. Financial support from the Spanish Ministry of Economy and Business via the ADaMANT (Computational Framework for Additive Manufacturing of Titanium Alloy) project (Proyectos de I + D (Excelencia) DPI2017-85998-P) is gratefully acknowledged.

References

Adams, B., Ebeida, M., Eldred, M., Jakeman, J., Swiler, L., Bohnhoff, W., Dalbey, K., Eddy, J., Hu, K., Vigil, D., Bauman, L.: DAKOTA: a multilevel parallel object-oriented framework for design optimization, parameter estimation, uncertainty quantification, and sensitivity analysis, version 5.3.1 reference manual. Technical Report, U.S. Department of Energy (2013)

Attaran, M.: The rise of 3-D printing: the advantages of additive manufacturing over traditional manufacturing. Bus. Horiz. **60**(5), 677–688 (2017)

Atzeni, E., Salmi, A.: Economics of additive manufacturing for end-usable metal parts. Int. J. Adv. Manuf. Technol. **62**(9–12), 1147–1155 (2012)

Bellini, A., Güçeri, S.: Mechanical characterization of parts fabricated using fused deposition modeling. Rapid Prototyp. J. **9**(4), 252–264 (2003)

Brenken, B., Barocio, E., Favaloro, A., Kunc, V., Pipes, R.B.: Fused filament fabrication of fiber-reinforced polymers: a review. Addit. Manuf. **21**, 1–16 (2018)

Cantrell, J.T., Rohde, S., Damiani, D., Gurnani, R., DiSandro, L., Anton, J., Young, A., Jerez, A., Steinbach, D., Kroese, C., Ifju, P.G.: Experimental characterization of the mechanical properties of 3D-printed ABS and polycarbonate parts. Rapid Prototyp. J. **23**(4), 811–824 (2017)

Casavola, C., Cazzato, A., Moramarco, V., Pappalettere, C.: Orthotropic mechanical properties of fused deposition modelling parts described by classical laminate theory. Mater. Des. **90**, 453–458 (2016)

Cervera, M., Agelet de Saracibar, C., Chiumenti, M.: COMET: Coupled Mechanical and Thermal Analysis, Data Input Manual, Version 5. 0, Technical Report IT-308 (2002). http://www.cimne.upc.es

Dadvand, P., Rossi, R., Oñate, E.: An object-oriented environment for developing finite element codes for multi-disciplinary applications. Arch. Comput. Methods Eng. **17**(3), 253–297 (2010)

Delfs, P., Tows, M., Schmid, H.J.: Optimized build orientation of additive manufactured parts for improved surface quality and build time. Addit. Manuf. **12**, 314–320 (2016)

Domingo-Espin, M., Puigoriol-Forcada, J.M., Garcia-Granada, A.A., Llumà, J., Borros, S., Reyes, G.: Mechanical property characterization and simulation of fused deposition modeling Polycarbonate parts. Mater. Des. **83**, 670–677 (2015)

Durgun, I., Ertan, R.: Experimental investigation of FDM process for improvement of mechanical properties and production cost. Rapid Prototyp. J. **20**(3), 228–235 (2014)

Garg, A., Bhattacharya, A.: An insight to the failure of FDM parts under tensile loading: finite element analysis and experimental study. Int. J. Mech. Sci. **120**, 225–236 (2017)

Gibson, I., Rosen, D.W., Stucker, B.: Additive Manufacturing Technologies: Rapid Prototyping to Direct Digital Manufacturing. Springer, New York (2010)

Gray, R.W., Baird, D.G., Helge Bøhn, J.: Effects of processing conditions on short TLCP fiber reinforced FDM parts. Rapid Prototyp. J. **4**(1), 14–25 (2002)

Guo, N., Leu, M.C.: Additive manufacturing: technology, applications and research needs. Front. Mech. Eng. **8**(3), 215–243 (2013)

Hill, R.: Elastic properties of reinforced solids: some theoretical principles. J. Mech. Phys. Solids **5**(11), 357–372 (1963)

Hill, R.: A self-consistent mechanics of composite materials. J. Mech. Phys. Solids **13**(4), 213–222 (1965)

Kotlinski, J.: Mechanical properties of commercial rapid prototyping materials. Rapid Prototyp. J. **20**(6), 499–510 (2014)

Lloberas-Valls, O., Rixen, D.J., Simone, A., Sluys, L.J.: Domain decomposition techniques for the efficient modeling of brittle heterogeneous materials. Comput. Methods Appl. Mech. Eng. **200**(13), 1577–1590 (2011)

Lloberas-Valls, O., Rixen, D.J., Simone, A., Sluys, L.J.: Multiscale domain decomposition analysis of quasi-brittle heterogeneous materials. Int. J. Numer. Meth. Eng. **89**(11), 1337–1366 (2012)

Lourenço, P.B., Rots, J.G.: Multisurface interface model for analysis of masonry structures. J. Eng. Mech. **123**(7), 660–668 (1997)

Mandel, J.: Plasticité classique et viscoplasticité. Springer-Verlag, Berlin (1971)

McLouth, T.D., Severino, J.V., Adams, P.M., Patel, D.N., Zaldivar, R.J.: The impact of print orientation and raster pattern on fracture toughness in additively manufactured ABS. Addit. Manuf. **18**, 103–109 (2017)

Ngo, T.D., Kashani, A., Imbalzano, G., Nguyen, K.T., Hui, D.: Additive manufacturing (3D printing): a review of materials, methods, applications and challenges. Compos. B Eng. **143**, 172–196 (2018)

Nguyen, V.P., Stroeven, M., Sluys, L.J.: Multiscale continuous and discontinuous modeling of heterogeneous materials: a review on recent developments. J. Multiscale Model. **3**(04), 229–270 (2011)

O'Connor, H.J., Dickson, A.N., Dowling, D.P.: Evaluation of the mechanical performance of polymer parts fabricated using a production scale multi jet fusion printing process. Addit. Manuf. **22**, 381–387 (2018)

Olakanmi, E.O., Cochrane, R.F., Dalgarno, K.W.: A review on selective laser sintering/melting (SLS/SLM) of aluminium alloy powders: processing, microstructure, and properties. Prog. Mater Sci. **74**, 401–477 (2015)

Oller, S., Miquel Canet, J., Zalamea, F.: Composite material behavior using a homogenization double scale method. J. Eng. Mech. **131**(1), 65–79 (2005)

Otero, F., Martínez, X., Oller, S., Salomón, O.: Study and prediction of the mechanical performance of a nanotube-reinforced composite. Compos. Struct. **94**, 2920–2930 (2012)

Otero, F., Oller, S., Martinez, X., Salomón, O.: Numerical homogenization for composite materials analysis. comparison with other micro mechanical formulations. Compos. Struct. **122**, 405–416 (2015)

Peterson, A.M.: Review of acrylonitrile butadiene styrene in fused filament fabrication: a plastics engineering-focused perspective. Addit. Manuf. **27**, 363–371 (2019)

Sillani, F., Kleijnen, R.G., Vetterli, M., Schmid, M., Wegener, K.: Selective laser sintering and multi jet fusion: process-induced modification of the raw materials and analyses of parts performance. Addit. Manuf. **27**, 32–41 (2019)

Sood, A.K., Ohdar, R.K., Mahapatra, S.S.: Parametric appraisal of mechanical property of fused deposition modelling processed parts. Mater. Des. **31**(1), 287–295 (2010)

Sood, A.K., Ohdar, R.K., Mahapatra, S.S.: Experimental investigation and empirical modelling of FDM process for compressive strength improvement. J. Adv. Res. **3**(1), 81–90 (2012). https://doi.org/10.1016/j.jare.2011.05.001.23

Suquet, P.: Local and global aspects in the mathematical theory of plasticity. Plasticity Today 279–309 (1985)

Thrimurthulu, K., Pandey, P.M., Reddy, N.V.: Optimum part deposition orientation in fused deposition modeling. Int. J. Mach. Tools Manuf. **44**(6), 585–594 (2004)

Townsend, A., Senin, N., Blunt, L., Leach, R.K., Taylor, J.S.: Surface texture metrology for metal additive manufacturing: a review. Precis. Eng. **46**, 34–47 (2016)

Tymrak, B.M., Kreiger, M., Pearce, J.M.: Mechanical properties of components fabricated with open-source 3-D printers under realistic environmental conditions. Mater. Des. **58**, 242–246 (2014)

Yang, Q., Li, H., Zhai, Y., Li, X., Zhang, P.: The synthesis of epoxy resin coated Al2O3 composites for selective laser sintering 3D printing. Rapid Prototyp. J. **24**(6), 1059–1066 (2018)

Zaldivar, R.J., Witkin, D.B., McLouth, T., Patel, D.N., Schmitt, K., Nokes, J.P.: Influence of processing and orientation print effects on the mechanical and thermal behavior of 3D Printed ULTEM® 9085 Material. Addit. Manuf. **13**, 71–80 (2017)

Ziemian, C.W., Ziemian, R.D., Haile, K.V.: Characterization of stiffness degradation caused by fatigue damage of additive manufactured parts. Mater. Des. **109**, 209–218 (2016)